Terahertz absorption of illuminated photosynthetic reaction center solution: a signature of photoactivation?

Terahertz Absorption of illuminated Photosynthetic Reaction Center solution: a signature of photoactivation?

Ida Lundholm[a], Weixiao Y. Wahlgren[a], Federica Piccirilli[b,c,d], Paola Di Pietro[b], Annette Duelli[a], Oskar Berntsson[a], Stefano Lupi[e], Andrea Perucchi[b] and Gergely Katona[a*]

Abstract

Photosynthetic reaction centers develop a stable charge separated state upon illumination. To investigate the molecular vibrations associated with the illuminated state of a reaction center we recorded terahertz absorption spectra of the photosynthetic reaction center from *Rhodobacter sphaeroides* in the dark and upon illumination and observed a small, but significant THz absorption increase in the 20 to 130 cm^{-1} spectral region. Reaction centers show very similar terahertz absorption increase when solubilized in detergents and in a lipidic sponge phase indicating that the nature of the bulk solvent has limited influence on the vibrational spectrum. The absorption change of the isolated LM subunit is very similar to that of the intact reaction center. Through temperature control experiments we show that 89 % of the absorption change is likely attributed to the non-thermal activation of the protein molecules. These results indicate that picosecond molecular vibrations change primarily in the cofactors and/or in the evolutionary conserved core of the reaction centre upon illumination, whereas the nuclear motions of the H-subunit and the bulk solvent have limited impact on the terahertz spectral changes.

Introduction

Most energy enters into the biosphere through reaction center based photosynthesis. The photosynthetic reaction centers are membrane proteins, which play an important role in converting solar energy into chemical energy. Reaction centers from very different organisms share common architecture such as having (pseudo-) dimeric core subunits embedded in the membrane with a symmetric set of cofactors through which electrons travel from one side of the membrane to the other. As illustrated in Figure 1A the reaction center from *Rhodobacter sphaeroides (R. sphaeroides)*(RC_{sph}) is comprised of a H (heavy), L (light) and M (medium) subunit, which orients cofactors for an electron transfer chain. Figure 1B highlights the highly symmetrical arrangement of the cofactors: 2 bacteriochlorophylls forming a special pair (P_{870}), 2 accessory bacteriochlorophylls, 2 bacteriopheophytins, a tightly bound ubiquinone (Q_A) and a mobile ubiquinone (Q_B) not showed in the figure. Upon illumination the reaction center absorbs one photon and one electron of the excited special pair is transferred through the bacteriopheophytin to Q_A. The electron is transferred further to the Q_B site if a ubiquinone is bound at the site. In the absence of an external electron donor or acceptor the reaction center returns to the ground state through charge recombination either from the $P^+Q_A^-$ or $P^+Q_B^-$ state.

The charge separated state of the reaction center is remarkably long lived compared to synthetic models of photosynthesis[1]. The lifetime of the $P^+Q_A^-$ state also depends on whether the reaction center was dark adapted or exposed to continuous illumination. Kinetic, biochemical and X-ray crystallographic evidence shows that continuous exposure to bright light changes the protein structure[2-6].

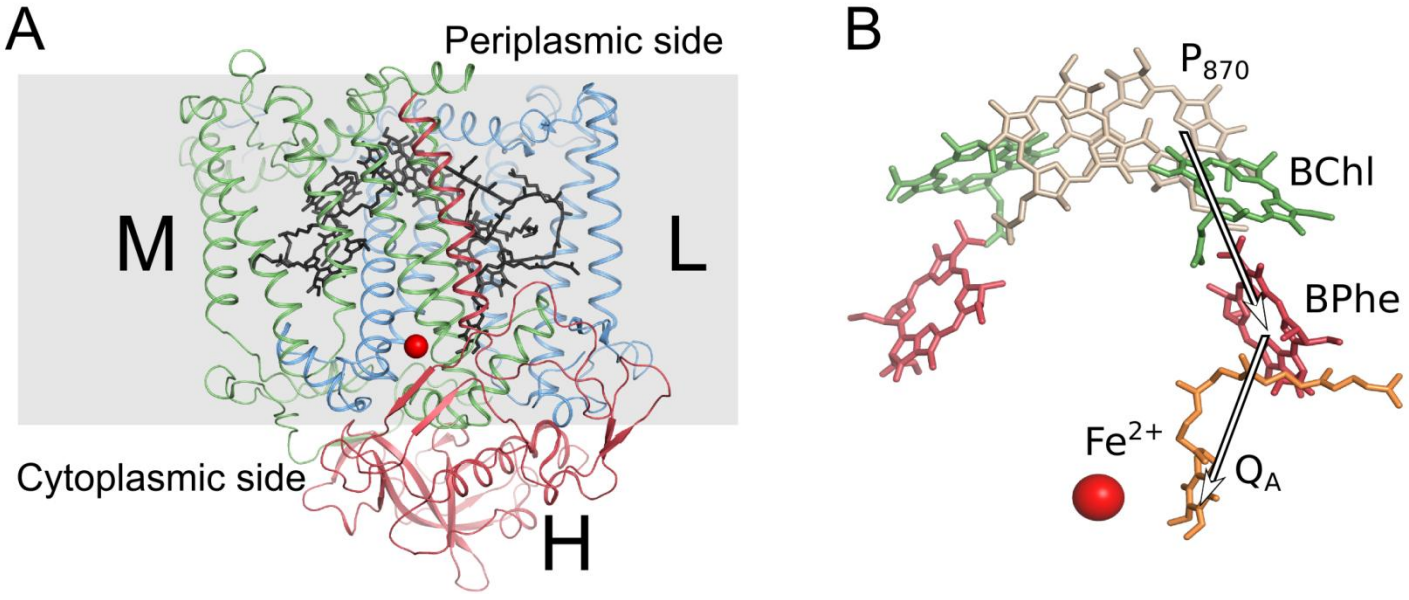

Figure 1A. Structure of the photosynthetic reaction center form *R. sphaeroides* (PDB ID 2BNP) showing the three subunits M (green), L (blue) and H (red) and the cofactors (black). The gray region of the picture shows the membrane embedded part of the protein. B. Cofactors of the reaction center, the special pair(P_{870}), bacteriochlorophyll(BChl), bacteriopheophytin(BPhe) and the bound quinone (Q_A). The electron transfer pathway through the cofactors that leads to the charge separated state, $P_{870}^{+}\ Q_A^{-}$, is shown by the arrows.

Although these structural studies provide valuable insights into the conformational changes occurring in dark adapted reaction centers different mechanisms may increase the lifetime of the charge stabilized state in light adapted reaction centers by three orders of magnitudes. These mechanisms may include conformational changes in the charge separated state and increased penetration of the solvent into the protein structure[3]. It has been proposed that a conformational change of a helix in the H-subunit is mainly responsible for the charge stabilization[3]. However, in a conventional detergent grown crystal form of reaction center from *Rhodopseudomonas viridis* no obvious conformational change was found [7]. In lipidic cubic/sponge phase grown crystals[8-10] the structure is affected differently by crystal contacts and the corresponding conformational changes can develop. Although the intermediate trapping was performed at cryogenic temperature, there was a good agreement with the observed difference electron density features and the changes in cleavage sites susceptible to limited proteolysis at room temperature upon extended light illumination[11]. Susceptibility to proteolysis is facilitated by the increased dynamics of the substrate since the surrounding residues of the scissile bond often have to adapt to an antiparallel β-sheet conformation when bound to the protease active site[12, 13]. In addition, the temperature dependence of charge recombination kinetics provided further circumstantial evidence for protein motions being important during functional changes upon extended illumination[14].

Marcus theory assume that the vibrations coupled to the electron transfer have the same frequency in starting and product states, which also implies that there is no entropy change in electron transfer reactions.[15] In reality the entropic contribution may constitute about half of the free energy difference between the ground and the charge separated state.[16] The entropic contribution is surprisingly positive despite of the assumed ordering of dipoles around the newly formed charges. It is increasingly recognized that vibrational motions are important in photosynthetic electron transport[17], but the molecular dynamics simulations may not fully account for the true dynamics in reaction centers. Ultrafast pump probe experiments probe the response of the cofactors immediately following photoexcitation and give valuable insight into nuclear motions of the cofactors and their immediate surroundings[18] and

identified 15 cm^{-1} and 77 cm^{-1} modes in RC_{sph} arising from the protein matrix.

The contribution of very low-frequency collective vibrations (occurring still on ps timescales) contribute significantly to the entropy of the system[19] and the ubiquitous presence of the entropy term influences not only electron transport rates, but also the catalytic power of enzymes and protein:protein recognition. It appears to make a lot of sense to directly study the low frequency vibration spectrum of the photoactivation of RC. Why is this not a common practice? One reason is that it is difficult to produce and detect terahertz (THz) radiation which corresponds to the spectral region of protein vibrations and the THz absorption of proteins is difficult to separate from that of the solvent. Absorption of a sample *decreases* with increasing protein concentration as protein molecules displace water molecules in the sample. [20] Despite of the challenges in producing and detecting THz radiation, THz spectroscopy has already proven to be a suitable technique for studying protein dynamics. Pioneering THz absorption spectroscopy on proteins have been done in dehydrated [21] and in aqueous [20, 22-26] environments. The obtained THz spectra are often difficult to interpret due to the large number of overlapping spectral bands originating from the solvent and the protein[20]. On the other hand the native environment of proteins is aqueous and the solvent environment is thought to drive protein motions. [27, 28] Light activation of bacterierhodopsin and photoactive yellow protein have been studied [22, 24], where the difference spectrum between the illuminated and the dark state of the sample removes the contribution of the light-insensitive bulk solvent. In this study we show that it is possible to detect extremely small THz absorption changes (as little as 0.005% change in the total signal) by applying a self referencing methodology using synchrotron THz radiation. In addition to measurements on the intact reaction center we investigated how the evolutionary conserved core of the reaction center, the L and M subunit, responds to continuous illumination in the absence of the H-subunit. To explore the role of the bulk solvent on THz difference spectra of the protein we performed the experiments both on detergent and lipidic sponge phase solubilized reaction centers.

Materials and Methods

Sample preparation

Reaction centers from *R. sphaeroide*s strain R-26 were cultured and purified as described previously [29]. Purified RC_{sph} were concentrated to a final concentration of 0.76 mM and 1.1 mM in buffer (0.1M HEPES pH 8.1, 250 µM terbutryn and 0.1% LDAO).

The LM complex of reaction center from *R. sphaeroide*s strain R-26 (LM_{sph}) were isolated with the chaotropic agent $LiClO_4$ based on the method described by Debus and coworkers [30]. Purified RC_{sph} with A_{802}=10 were incubated for 1 h at 25 °C in 0.75 M $LiClO_4$, 50 mM $CaCl_2$, 10 % (v/v) ethanol, 15 mM Tris pH 8.0, 0.1 mM EDTA and 0.1 % LDAO. Precipitated H-subunits were removed by centrifugation and the supernatant were dialyzed for 20 h in 100 mM HEPES pH 8.1 and 0.1 % LDAO at 4 °C. The dialyzed LM complex solution were finally concentrated to 0.2 mM (determined with ε_{802}=288 $cm^{-1}mM^{-1}$) and stored in -80 °C after flash freezing in liquid N_2. The success of the H-subunit removal was controlled with SDS-PAGE (Figure S1). Prior to measurements the LM complexes were concentrated to a final concentration of 0.71 mM in buffer (0.1M HEPES pH 8.1, 250 µM terbutryn and 0.1% LDAO).

Sponge phase were prepared based on a method described previously [10]. Firstly a cubic phase was prepared by mixing monoolein with a 0.1 M HEPES pH 8.1 and 0.1% LDAO buffer in a ratio of 60:40. The cubic phase was then mixed 1:4 with precipitant solution containing the swelling agent Jeffamine M600 (1 M HEPES pH 8.1, 20 % Jeffamine M600, 0.7 M $(NH_4)_2SO_4$) and the solution were incubated over night at room temperature resulting in a phase separation, the sponge phase was then harvested from the upper phase. RC_{sph} sponge phase samples were prepared by mixing 0.76 mM RC_{sph} (prepared as described previously) with sponge phase in a 1:1 ratio. The water content of the protein samples and the sponge phase was determined by comparing the sample weight before and after complete water evaporation in vacuum.

THz spectroscopy

THz absorption spectra were recorded at the SISSI beamline at the Elettra synchrotron [31]. The SISSI synchrotron source collects synchrotron light from bending magnet 9.1. The beamline then propagates all the radiation frequencies from THz to the visible range. The frequency spectrum of the SISSI synchrotron source is therefore white between 10 and 20000 cm^{-1} (0.3 - 600 THz).

The coupling of the SISSI beamline with the Bruker VERTEX 70v Spectrometer is achieved through a custom made adaption box, comprising 4 off-axis parabolic mirrors. The last mirror has a focal length of 153 mm, thus matching the numerical aperture of the entrance of the spectrometer optics. Schematics of the beamline

design are shown in Figure S2 in the Supporting Material. The liquid cell containing the sample is mounted in the sample compartment of the Bruker spectrometer. In order to minimize THz absorption by vapor water the sample chamber were purged with dry N_2 gas during all measurements.

The spectral content of the radiation used in our experiment is determined by the combined absorptions of the Si beam splitter and of the wedged THz filter (CaF_2/quartz). This limits the recorded spectrum of synchrotron light into the 0-4 THz spectral range, as shown in Figure S3. In this region, synchrotron radiation power is estimated to be in the 0.1 mW range. This power is an estimate based on comparisons with conventional sources as direct measurement cannot be done with a FTIR spectrometer. At each position of the moving mirror all the power emitted by the source is present. This is a very important difference of FTIR with respect to spatially dispersing spectrometers, the so called Fellgett (or multiplex) advantage since it provides a significant advantage in terms of signal to noise ratio (proportional to the square root of the number of sampling positions).

The detector employed is a He cooled Si bolometer from IRLabs (Model no. HDL-8), such detectors are routinely used in far infrared FTIR set-ups. The small Si element is thermally bonded to a suitably blackened 2.5 mm diamond absorber mounted in a cylindrical cavity. A Winston cone collects THz radiation from the window of the dewar (PE), and guide it to the Si bolometer.

4 µl of sample was encapsulated between two Z-cut quartz windows separated by 25 µm with a Teflon spacer. The sealed sample was kept in a liquid cell which was temperature controlled to 25 ºC. A temperature-controlled liquid sample cell (from Harrick) was used to maintain the required temperature of the sample during the data collections. The quartz windows with the sample encapsulated were mounted in a stainless steel (type 316) cylinder with an inner diameter of 13 mm, outer diameter of 63 mm and height of 25.5 mm. The temperature of the stainless steel cylinder was controlled by a fluid heat exchange system and a thermocoupler was mounted on the sample holder near the quartz sample slides to monitor the temperature.

Samples of RC_{sph} and LM_{sph} were excited using a 532 nm continuous wave laser with an intensity of 7.7 kW/m^2 and a spot size of 0.2 cm^2 measured 15mm from the sample. The laser was arriving at the sample at a ~30° angle. Buffer solution and sponge phase without protein was also used in control experiments. The laser and the THz beam were simultaneously illuminating the sample. Transmitted THz spectra were recorded alternately from illuminated and non-illuminated samples for 70 s each with a 10 s delay between every measurement. The effect of temperature was monitored by recording THz spectra of a 0.76 mM RC_{sph} sample at 25 °C and 26 °C alternately. The temperature was cycled between 25 °C and 26 °C five times and 10 spectra were recorded at each temperature with at least 30 min of equilibration time between temperature change and the start of the acquisition. Each spectrum was collected for 70s. Due to instabilities in the detector and the THz beam 10 spectra from each temperature were picked out to be used in the analysis.

The difference absorbance, ΔA, was calculated according to:

$$\Delta A = -\log\left(\frac{I_{light}}{I_{dark}}\right) \qquad (1)$$

where I_{light} is the THz radiation transmitted by the illuminated protein sample and I_{dark} the THz radiation transmitted by the non illuminated protein sample. Difference absorbance coefficients were calculated by dividing the difference absorbance with the path length (25µm).

As a spectral similarity measure the RMSD between two spectra were calculated according to:

$$RMSD = \left[\frac{\sum_{i=1}^{n}(S_{1,i}-S_{2,i})^2}{n}\right]^{\frac{1}{2}} \qquad (2)$$

Where $S_{1,i}$ and $S_{2,i}$ are two spectra at the *i*th frequency data point and *n* is the number of data points per spectrum.

Steady state temperature increase simulations

Comsol Multiphysics software was used to simulate the processes of heat transfer between the sample and the sample cell during the data collections [32]. Comsol is a Finite Element (FEM) Partial Differential Equation (PDE) solution software [33]. During the simulation, partial differential equation of heat conduction in solid was used with Cartesian coordinates. The initial temperature of the system was set to 298.15 K and a constant surface temperature of 298.15 K at the stainless cylinder inner surface was modeled as the boundary condition. The theoretical absorption energy of the green laser by the RC sample was calculated using the UV/VIS spectroscopy and was estimated to be 24.6 % of the total laser power. The loss of the laser radiation by the reflection of the first quartz window and the partial laser beam due to the angle of the incoming laser beam relative to the sample was taken into account. A total power of 0.002W at 0.76

mM protein concentration with a beam size of 8.0 mm in diameter was modeled on the sample which was treated as water.

UV/VIS spectroscopy

Optical absorption spectroscopy was performed with a 4DX microspectrophotometer [34]. 2µl RC_{sph} sample was placed between two Z-cut quartz windows separated by a 25 µm Teflon spacer. Spectra were recorded in the dark and under illumination of a 532nm laser with intensity 7.7 kW/m^2.

Elastic network modeling

Elastic network models can substitute detailed atomic models traditionally used in molecular simulations by incorporating much fewer parameters, while still retaining specific interaction patterns. They are expected to perform best when simulating low frequency, elastic, delocalized normal modes which occur in the THz region, while simulation of localized intra residue vibrations require all atomic models or quantum chemical simulations. A great advantage of elastic network models is that they do not require computationally expensive and inaccurate energy minimization steps permitting direct analysis of crystal structures.[35]

Low frequency normal modes were simulated using stand alone programs (PDBMAT and DIAGRTB) from the ElNemo package based on crystal structures of RC_{sph} [36]. PDBMAT were used to calculate the Hessian matrix from the crystal structures given the strength of the springs, specified by the force constant, connecting interacting atoms in the structure as defined by the Tirion step function [35]. Masses were defined individually for each atom. The force constant of interacting atoms was identical for all parts of the protein in a given model. To obtain the eigenvectors corresponding to the low frequency normal modes of the system the Hessian matrix were diagonalized using the program DIAGRTB. DIAGRTB assumes that each amino acid in the structure behaves as a rigid body, which is a useful approximation for large systems.

The normal modes of RC_{sph} were calculated for the crystal structure from a non-illuminated (PDB ID 2BNP) [37] sponge phase grown crystal.

Result and Discussion

Solutions of RC_{sph} were probed with synchrotron based THz radiation and compared to the same sample illuminated with green laser light (532 nm). We estimated the fraction of activated reaction center molecules by UV/VIS spectroscopy with identical experimental design. The spectra were convoluted with a Gaussian function to remove the noise. The noise reduced UV/VIS absorption spectra of RC_{sph} with and without laser illumination are presented in Figure 2. Upon illumination the reaction center molecules are in a photostationary state with a fraction of molecules in the charge separated state. In the charge separated state the absorption peak at 855 nm is decreased compared to the ground state because the absorption of the positively charged special pair is quenched. By comparing the height of the absorption peaks at 855 nm in the illuminated and the ground state the fraction of charge separated RC_{sph} were estimated to be 33% for a laser intensity of 7.7 kW/m^2. This light intensity was necessary to populate a sufficiently high fraction of charge separated states.

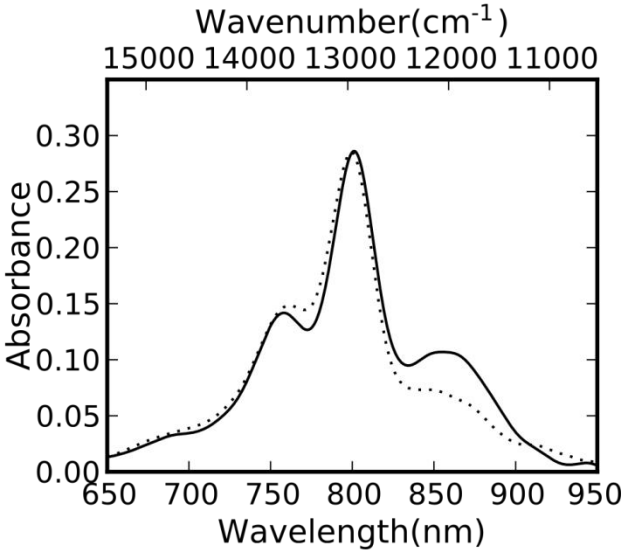

Figure 2 Optical absorption spectra of 0.62 mM reaction center solution in ground state (solid line) and illuminated by 7.7 kW/m^2 (dotted line).

Due to the high absorbance of water in the THz frequency region it is very challenging to extract the absolute spectrum for the reaction center. On the other hand the difference between light adapted and ground states of RC_{sph} and LM_{sph} can be studied through their difference absorbance spectra. Figure 3 shows the difference THz absorbance coefficient spectra between the light activated and dark state of RC_{sph}, LM_{sph} (Figure 3A) and RC_{sph} reconstituted into sponge phase (Figure 3B). The experimental data shows an increased absorption coefficient for all protein samples compared to both the buffer solution and the pure sponge phase. The most reliable feature

of the difference absorbance coefficient spectrum is a broad local maximum at 90-100 cm^{-1}, which is present in all protein difference spectra. Higher protein concentration and higher light intensity generally gives higher difference signal as the population of the light activated state increases. Interestingly, the difference absorbance signal of RC_{sph} is independent of the detergent or lipidic environment. The smaller difference absorbance signal for the sponge phase/protein mixture is due to the dilution of RC_{sph} when reconstituting it into sponge phase. Both the buffer and the sponge phase display a difference absorbance around zero over the whole spectral region when RC_{sph} is not present showing the exceptional stability of the experimental setup and that the bulk solvent is not directly affected by the laser.

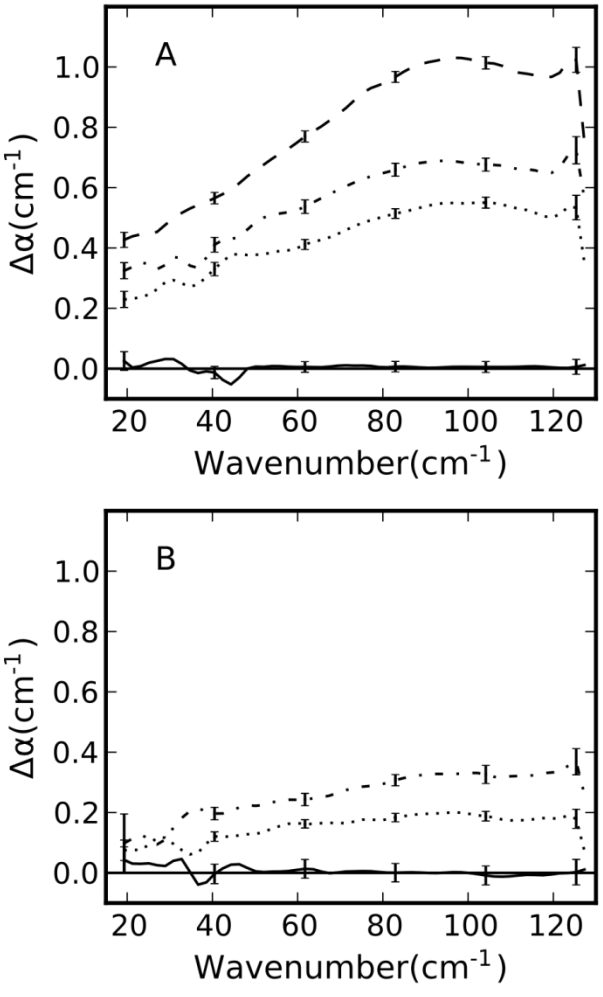

Figure 3 Difference in THz absorption ($\alpha_{illuminated}$-α_{ground}) of RC_{sph} and LM_{sph} in detergent (A) and sponge phase (B) illuminated with laser intensity 7.7 kW/m^2. The error bars are representing the standard error ($\sigma / \sqrt{N}$). In A the two upper spectra are recorded from two different concentrations of RC_{sph}, 1.1 mM (dashed line), an average of 86 difference absorbance spectra and 0.76 mM (dash-dot line), an average of 90 difference absorbance spectra. The spectrum represented as the dotted line shows the difference absorption of the LM_{sph} complex collected from two different samples with a concentration of 0.71 mM, in total 87 difference absorbance spectra. The spectrum represented by a solid line shows the difference absorbance for detergent based buffer, an average of 59 difference absorbance spectra. In B the two upper spectra shows the difference absorbance for RC_{sph} (0.76 mM) mixed 1:1 with sponge phase, the spectrum represented as a dash dot line is collected from a sample mixed directly prior to measurement (average of 141 spectra) while the spectrum represented as a dotted line is collected from a sample that were incubated for 14 days in RT (an average of 92 spectra). The spectrum represented as a solid line is collected from pure sponge phase, an average of 42 difference absorbance spectra.

The difference absorbance of LM_{sph} is lower than that of $RC_{sph,}$ but the shape of the curves are not different. LM_{sph} and RC_{sph} has in these experiments almost the same molar concentration, but when taking into account that the occupied volume of RC_{sph} in solution is 1.44 times larger than for LM_{sph} the difference absorbance for LM_{sph} turns out to be slightly larger than that of RC_{sph}. This implies that it is the LM_{sph} subunits that give rise to the spectral feature we see in the THz region upon extended illumination and that the H-subunit exerts a minor or no influence. After superposition of the light and dark adapted structures, 2BNS and 2BNP, of RC_{sph} the rmsd of all Cα atoms is 0.210 Å while it is 0.290 Å and 0.167 Å for the H-subunit and LM-subunits, respectively. Although mostly the H-subunit is affected in the crystal structures, the changes are also spread out in the LM subunit.

The rmsd of two normalized spectra of RC_{sph} from two different batches is about 0.02, and the rmsd of RC_{sph} in detergent versus in sponge phase is about 0.03. Comparing normalized LM_{sph} spectra with RC_{sph} gives an rmsd of about 0.03, thus more or less the same resemblance as between two independently recorded RC_{sph} spectra. Non-normalized RC_{sph} spectra and LM_{sph} spectra scaled to the same volumetric concentration results in an rmsd of 0.06, slightly higher because the overall spectral density is higher for LM_{sph} than for RC_{sph}.

Furthermore it also appears that the difference THz spectrum is largely insensitive to the solvent environment. This may seem to

contradict the solvent slaving model of protein dynamics, but one has to keep in mind that the reaction catalyzed by photosynthetic reaction centers is an extreme case which do not require thermal activation in contrast to many enzymatic reactions [27]. Instead the reaction center needs to dissipate the absorbed photon energy to the solvent.

The THz absorption of water is temperature dependent and at 33cm^{-1} a 1°C temperature increase would increase the absorption of approximately 4 cm^{-1} [38]. Using the program Comsol the temperature increase in the sample over one spectral acquisition was simulated[32]. The calculated steady state temperature profiles are shown in Figure 4. A temperature increase of about 0.09 °C is anticipated at the center of the sample and 0.07 °C at the side. The maximum temperature increase was predicted to be 0.13 K and 0.05 K for 1.1 mM and 0.38 mM RC_{sph} solutions, respectively. In these calculations we neglected radiative and convective heat dissipation.

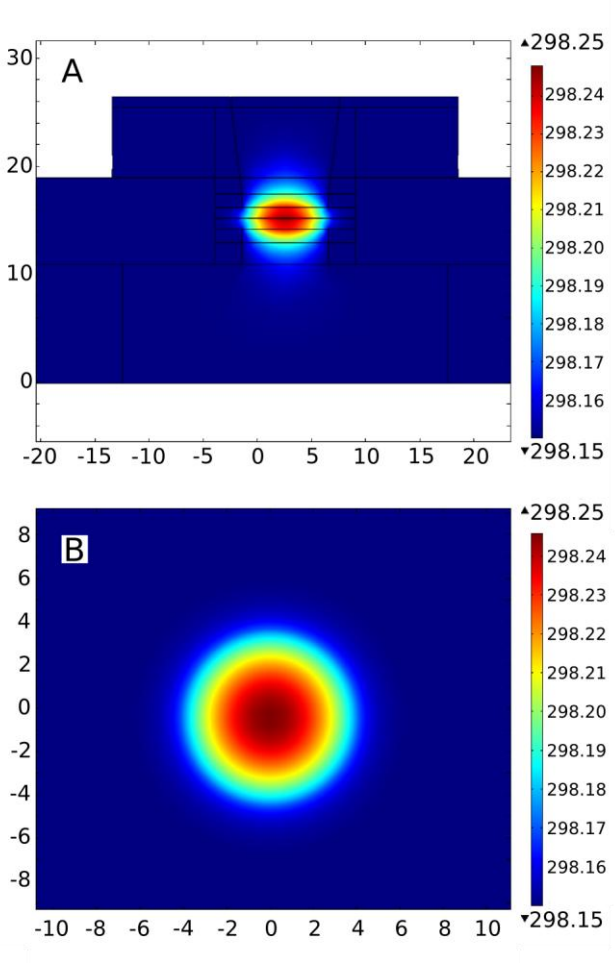

Figure 4 Calculated thermal profiles: (A) shows the side and (B) the top view of the steady-state thermal profile near the center of the sample in the presence of the irradiation from the laser. The colors indicate the temperature in Kelvin and distance units are in mm.

A protein sample cannot be approximated as a pure water sample so therefore the difference THz signal was investigated upon a temperature increase of 1 °C. In Figure 5 the difference absorbance signal is calculated between data sets recorded at sample temperatures of 25 °C and 26 °C and compared to the difference signal from laser activated RC_{sph}. Even a 1 °C temperature increase does not fully account for the THz absorption increase seen upon light activation indicating that the recorded signal is not primarily of thermal origin. Qualitative differences are also apparent, for example the laser induced absorption change is positive in the entire frequency range while the temperature induced changes are close to zero in the 40-50 cm^{-1} range.

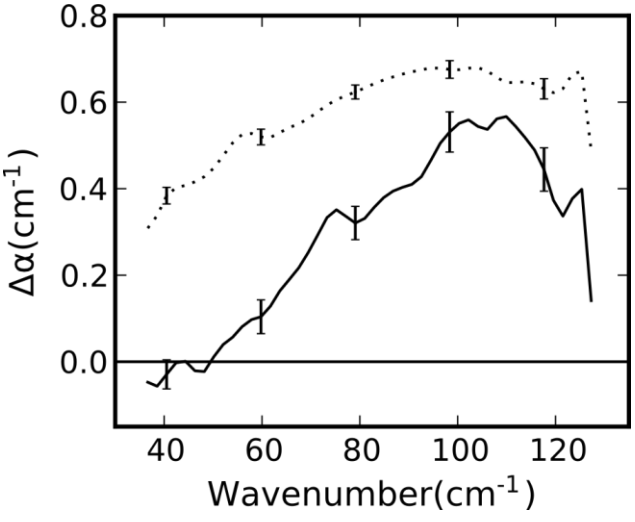

Figure 5. The difference absorption between spectra measured at sample temperatures of 25°C and 26°C (solid line). 10 spectra were used from each temperature when calculating the difference absorbance and the sample used was 0.76mM RC_{sph} in detergent. This 1 °C temperature difference is about ten times higher than the estimated temperature increase upon laser illumination. The difference absorbance spectra for the 0.76 mM RC_{sph} sample illuminated with a 7.7kW/m^2 laser is shown as a dotted line for comparison. The error bars are representing the standard error ($\sigma / \sqrt{N}$).

In Figure 6 three of the difference THz absorbance spectra collected from 0.76 mM and 1.1 mM RC_{sph} in detergent and 0.38 mM RC_{sph} in sponge phase samples are scaled according to their protein concentration. It is clear that the concentration is directly

proportional to the intensity of the signal and that the signal is not substantially affected by the type of solvent. In the different samples used in this study the water content varies, a 0.76 mM RC_{sph} solution contains 62 % (w/w) water and a 1.1 mM RC_{sph} solution 49 % (w/w) water. Pure sponge phase contains 25 % (w/w) water and thus the water content of the RC_{sph} sample in sponge phase has a water content of 43 %. When comparing the different samples, the magnitude of the THz difference signal does not show any correlation with the water content.

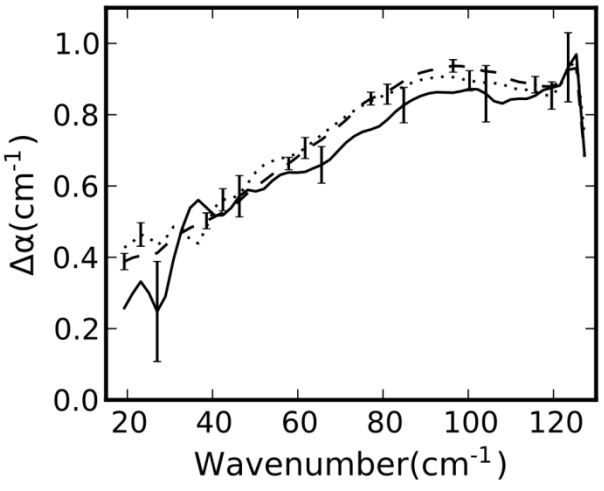

Figure 6. Difference in THz absorption ($\alpha_{illuminated}$-α_{ground}) of 1.1 mM RC_{sph} (dashed line) and 0.76 mM RC_{sph} (dotted line) in detergent and 0.76 mM RC_{sph} mixed 1:1 with sponge phase (solid line) illuminated with laser intensity 7.7 kW/m^2 , same spectra as are shown in Figure 3. The error bars are representing the standard error ($\sigma / \sqrt{N}$). The three spectra are scaled to a protein concentration of 1 mM.

Buried water molecules and those belonging to the first solvation layer are usually ordered, strongly bound to the protein and may well play a role in the THz absorption increase since their dynamic behavior is likely to be strongly coupled. There are no studies of absorption of detergents and lipidic sponge phases in the THz region. Since the control measurements on detergent solutions and lipidic sponge phase resulted in no difference in THz absorption it is unlikely that light activation has a direct effect on the vibration modes of the bulk solvent. Likewise fluctuations in sample temperature and THz radiation intensity do not introduce significant shift in the averaged difference THz absorption spectrum.

Qualitatively the observed absorption increase is similar to what happened upon the light induced activation of photoactive yellow protein. [22] The THz absorption increase appears to be associated with the components of the LM complex and the corresponding vibration density increase is in line with the positive entropy term associated with the photoinduced charge separation.[16] When considering the different components of the LM complex a bacteriochlorophyll monomer is too small to possess intrachromophore vibration modes below 130 cm^{-1}. [19, 39] Modes at 36, 94 and 127 cm^{-1} were observed for reaction center using shifted excitation difference resonance Raman spectroscopy corresponding to the special pair vibrations. [39] Solvated bacteriochlorophyll molecules also have intermolecular solvent modes at lower wavenumbers and similar vibrations can be expected in photosynthetic reaction centres.[40] On the other hand if the oxidized special pair would be solely responsible for the difference THz spectrum, one would expect changes in a few isolated IR active peaks, rather than the broad featureless absorption increase.

In an attempt to rationalize the increase in THz absorption in the 20 cm^{-1} to 130 cm^{-1} range we calculated the vibrational normal modes of RC_{sph} using an elastic network model [3, 8] (Figure 7). From this calculation we used the frequency normal modes which fell in the experimental spectral range and the first six normal modes corresponding to translation and rotational movements of the protein were excluded. As this crude model shows the normal mode density increases with frequency which is also typically observed in normal mode analysis of all atom protein models. As many normal mode calculations concluded the shape of the normal mode density qualitatively agrees with the THz spectrum of proteins. Therefore assuming that the density of normal modes increases from low to high frequencies, what may an increased THz absorption mean? One plausible explanation is that the normal mode density is red-shifted in the illuminated state of the protein, leading to an overall increase of normal mode density in the equivalent frequency ranges. In a qualitative model such as ENM a red shift can be caused by the weakening of the force constants in the model.

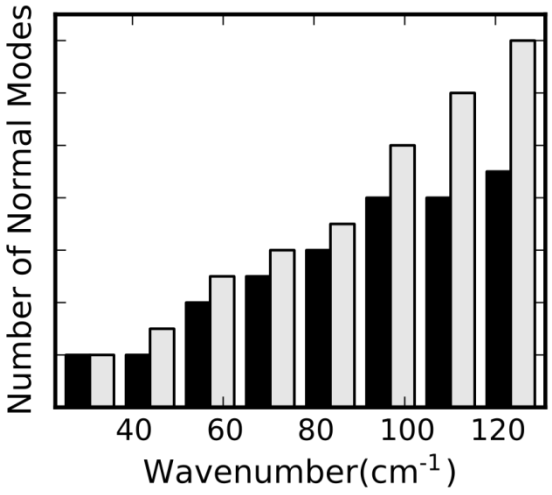

Figure 7. Histogram showing the number of calculated normal modes in the experimental spectral range, black bars showing a total of 44 normal modes, calculated with a force constant of 1.0 and grey bars showing a total of 56 normal modes calculated with a force constant of 0.8. The structure with PDB id 2BNP was used in the normal mode calculation.

Conclusion

Terahertz absorption spectroscopy has been used to determine changes in the vibrational spectrum of a reaction center upon photoinduced charge separation. We demonstrated that synchrotron based THz sources combined with self referencing data collection strategy can achieve extreme sensitivity and as little as 0.005% change in THz absorbance can be detected. In situ extended illumination of photosynthetic reaction centers increased the THz absorption of the sample in the 20-130 cm^{-1} range. By comparing difference THz absorption spectra from RC_{sph} solubilized in both detergent and lipidic sponge phase it appears that the absorption profile is independent of the surrounding solution and correlate well with the protein concentration. The THz absorption increase is associated with the chromophore containing LM complex and the increased low frequency vibrational activity is in line with the positive entropic stabilization of the light induced charge separated state.

Acknowledgements

The authors thank Yves-Henri Sanejouand and András Málnási-Csizmadia for the valuable discussions. These experiments were performed on the SISSI beamline at Elettra, Trieste, Italy. This work was supported by the Swedish Research Council.

Notes and References

[a] Department of Chemistry and Molecular Biology, University of Gothenburg, Gothenburg, Sweden

[b] INSTM UdR Trieste-ST and Sincrotrone Trieste S.C.p.A., Basovizza, Trieste, Italy

[c] Physics Department of Università degli studi di Trieste, Trieste, Italy

[e] CNR–IOM and Dipartimento di Fisica University of Rome "La Sapienza", Rome, Italy

[d] Current adress: Dipartimento Fisica e Chimica, Università degli Studi di Palermo, Palermo, Italy

*Corresponding author: gergely.katona@cmb.gu.se

I. Lundholm and W.Y. Wahlgren contributed equally to this work.

Electronic Supplementary Information (ESI) available: [Figures S1. SDS PAGE gel from LM purification, S2. Schematic description of the SISSI beamline and S3. Spectrum of recorded THz radiation at the SISSI beamline with the described detector configuration]. See DOI: 10.1039/b000000x/

1. M. R. Wasielewski, *Chem. Rev.*, 1992, **92**, 435-461.
2. U. Andreasson and L. E. Andreasson, *Photosynth. Res.*, 2003, **75**, 223-233.
3. G. Katona, A. Snijder, P. Gourdon, U. Andreasson, O. Hansson, L. E. Andreasson and R. Neutze, *Nat. Struct. Mol. Biol.*, 2005, **12**, 630-631.
4. V. N. Kharkyanen, Y. M. Barabash, N. M. Berezetskaya, E. P. Lukashev, P. P. Knox and L. N. Christophorov, *Chem. Phys. Lett.*, 2011, **512**, 113-117.
5. F. van Mourik, M. Reus and A. R. Holzwarth, *Biochim. Biophys. Acta*, 2001, **1504**, 311-318.
6. L. Kalman and P. Maroti, *Biochemistry*, 1997, **36**, 15269-15276.
7. R. H. Baxter, B. L. Seagle, N. Ponomarenko and J. R. Norris, *Acta Crystallogr. D*, 2005, **61**, 605-612.
8. G. Katona, U. Andreasson, E. M. Landau, L. E. Andreasson and R. Neutze, *J. Mol. Biol.*, 2003, **331**, 681-692.
9. P. Wadsten, A. B. Wohri, A. Snijder, G. Katona, A. T. Gardiner, R. J. Cogdell, R. Neutze and S. Engstrom, *J. Mol. Biol.*, 2006, **364**, 44-53.
10. A. B. Wohri, W. Y. Wahlgren, E. Malmerberg, L. C. Johansson, R. Neutze and G. Katona, *Biochemistry*, 2009, **48**, 9831-9838.
11. I. A. Smirnova, A. Blomberg, L. E. Andreasson and P. Brzezinski, *Photosynth. Res.*, 1998, **56**, 45-55.
12. K. Fodor, V. Harmat, R. Neutze, L. Szilagyi, L. Graf and G. Katona, *Biochemistry*, 2006, **45**, 2114-2121.
13. W. Y. Wahlgren, G. Pal, J. Kardos, P. Porrogi, B. Szenthe, A. Patthy, L. Graf and G. Katona, *J. Biol. Chem.*, 2011, **286**, 3587-3596.

14. B. H. McMahon, J. D. Muller, C. A. Wraight and G. U. Nienhaus, *Biophys. J.*, 1998, **74**, 2567-2587.
15. R. A. Marcus and N. Sutin, *Biochimica Et Biophysica Acta*, 1985, **811**, 265-322.
16. G. J. Edens, M. R. Gunner, Q. Xu and D. Mauzerall, *Journal of the American Chemical Society*, 2000, **122**, 1479-1485.
17. I. A. Balabin and J. N. Onuchic, *Science*, 2000, **290**, 114-117.
18. M. H. Vos, F. Rappaport, J.-C. Lambry, J. Breton and J.-L. Martin, *Nature*, 1993, **363**, 320-325.
19. N. Go, T. Noguti and T. Nishikawa, *Proc. Natl. Acad. Sci. U. S. A.*, 1983, **80**, 3696-3700.
20. J. Xu, K. W. Plaxco and S. J. Allen, *J. Phys. Chem. B*, 2006, **110**, 24255-24259.
21. R. Balu, H. Zhang, E. Zukowski, J. Y. Chen, A. G. Markelz and S. K. Gregurick, *Biophys. J.*, 2008, **94**, 3217-3226.
22. E. Castro-Camus and M. B. Johnston, *Chem. Phys. Lett.*, 2008, **455**, 289-292.
23. A. Markelz, S. Whitmire, J. Hillebrecht and R. Birge, *Phys. Med. Biol.*, 2002, **47**, 3797-3805.
24. S. E. Whitmire, D. Wolpert, A. G. Markelz, J. R. Hillebrecht, J. Galan and R. R. Birge, *Biophys. J.*, 2003, **85**, 1269-1277.
25. S. Ebbinghaus, S. J. Kim, M. Heyden, X. Yu, M. Gruebele, D. M. Leitner and M. Havenith, *J. Am. Chem. Soc.*, 2008, **130**, 2374-2375.
26. T. Q. Luong, P. K. Verma, R. K. Mitra and M. Havenith, *Biophys. J.*, 2011, **101**, 925-933.
27. P. W. Fenimore, H. Frauenfelder, B. H. McMahon and F. G. Parak, *Proc. Natl. Acad. Sci. U. S. A.*, 2002, **99**, 16047-16051.
28. H. Frauenfelder, G. Chen, J. Berendzen, P. W. Fenimore, H. Jansson, B. H. McMahon, I. R. Stroe, J. Swenson and R. D. Young, *Proc. Natl. Acad. Sci. U. S. A.*, 2009, **106**, 5129-5134.
29. G. Feher and M. Y. Okamura, eds. R. K. Clayton and W. R. Sistrom, Plenum Press, N.Y., 1978.
30. R. J. Debus, G. Feher and M. Y. Okamura, *Biochemistry*, 1985, **24**, 2488-2500.
31. S. Lupi, A. Nucara, A. Perucchi, P. Calvani, M. Ortolani, L. Quaroni and M. Kiskinova, *J. Opt. Soc. Am. B*, 2007, **24**, 959-964.
32. R. W. Pryor, *Multiphysics modeling using COMSOL: A first principles approach*, Jones & Bartlett Publishers, 2009.
33. V. Suarez, J. Hernandez Wong, U. Nogal, A. Calderon, J. B. Rojas-Trigos, A. G. Juarez and E. Marin, *Applied radiation and isotopes : including data, instrumentation and methods for use in agriculture, industry and medicine*, 2013.
34. A. Hadfield and J. Hajdu, *J. Appl. Crystallogr.*, 1993, **26**, 839-842.
35. M. M. Tirion, *Phys Rev Lett*, 1996, **77**, 1905-1908.
36. K. Suhre and Y. H. Sanejouand, *Nucleic Acids Res.*, 2004, **32**, W610-614.
37. H. M. Berman, J. Westbrook, Z. Feng, G. Gilliland, T. N. Bhat, H. Weissig, I. N. Shindyalov and P. E. Bourne, *Nucleic Acids Res.*, 2000, **28**, 235-242.
38. C. Ronne, L. Thrane, P. O. Astrand, A. Wallqvist, K. V. Mikkelsen and S. R. Keiding, *J Chem Phys*, 1997, **107**, 5319-5331.
39. A. P. Shreve, N. J. Cherepy, S. Franzen, S. G. Boxer and R. A. Mathies, *Proc. Natl. Acad. Sci. U. S. A.*, 1991, **88**, 11207-11211.
40. K. R. Shelly, E. A. Carson and W. F. Beck, *J. Am. Chem. Soc.*, 2003, **125**, 11810-11811.